Journal of Volcanology and Geothermal Research 311 (2016) 170–182

Contents lists available at ScienceDirect

Journal of Volcanology and Geothermal Research

journal homepage: www.elsevier.com/locate/jvolgeores

Zircon xenocryst resorption and magmatic regrowth at El Chichón Volcano, Chiapas, Mexico

Brenda Pack [a], Axel K. Schmitt [a,*], Julie Roberge [b], Felipe Garcia Tenorio [c], Brian N. Damiata [d]

[a] Department of Earth, Planetary, and Space Sciences, University of California Los Angeles, Los Angeles, CA 90095, USA
[b] ESIA-Ticomán, Instituto Politecnico Nacional (IPN), Av. Ticomán #600, Mexico, D.F, Mexico
[c] Instituto de Geofísica, UNAM Campus Morelia, 58090, Michoacán, Mexico
[d] Cotsen Institute of Archaeology, University of California Los Angeles, 308 Charles E Young Drive West, Los Angeles, CA 90024, USA

ARTICLE INFO

Article history:
Received 3 November 2015
Accepted 13 January 2016
Available online 26 January 2016

Keywords:
Crustal assimilation
Magma chamber
Cathodoluminescence
SIMS
Geochronology
Volcanic arc

ABSTRACT

El Chichón volcano is the only active volcano located within the Chiapanecan Volcanic Arc in southern Mexico, which lies between the Trans-Mexican Volcanic Belt and the Central American Volcanic Arc. Previous studies have shown that ~12 eruptions have occurred at El Chichón within the last 8000 years, forming a complex of lava domes with a central crater and surrounding pyroclastic deposits. Here, we report the discovery of zircon in Holocene El Chichón rocks, which were analyzed by high spatial resolution imaging (color cathodoluminescence CCL) and isotopic (secondary ionization mass spectrometry SIMS) methods to resolve core and rim crystallization ages. Pumice samples from five proximal pyroclastic flow and fall-out deposits were collected based on published stratigraphy. Two of the samples were further (re-)classified by new ^{14}C dates. In addition, we sampled two lavas from the 1982 eruption and from remnants of the older Somma lava complex. Zircon crystals were dated using $^{230}Th/^{238}U$ disequilibrium (U–Th) and U–Pb geochronology. U–Th zircon ages fall between near eruption ages and ca. 84 ka, with overlapping ages in all samples. By contrast, zircon core U–Pb ages range between ca. 290 Ma and 1.9 Ga. These ages are consistent with xenocrystic origins and their heterogeneity indicates derivation from clastic country rocks. Strong age contrasts between inherited xenocrystic and young magmatic domains in individual zircon crystals are evidence for arrested assimilation of crustal rocks where initially zircon-undersaturated magmas cooled rapidly to form a crystal mush or subsolidus amalgamate as a crustally contaminated boundary layer. This layer contributed zircon crystals to eruptible magma during episodic recharge events followed by partial melt extraction, mixing and homogenization. Zircon overgrowths are significantly older than major minerals whose U-series ages and sharp zonation boundaries suggest crystallization only within a few ka before eruption. This implies that zircon can detect magmatic longevity which is obscured in the major mineral record.

1. Introduction

The volcanic eruption of El Chichón volcano (Chiapas, Mexico) in March 1982 was one of the most catastrophic volcanic disasters in the 20th century. When it awoke, venting of trachyandesitic magma generated pyroclastic flows, ash-falls, debris flows, and surges coeval with the explosive disintegration of an ~1 km diameter central dome (Rose et al., 1984). Ultimately, the eruption generated a new crater within an older depression, whose prominent topographic margin is known as the Somma rim (Rose et al., 1984). Distal tephra falls were deposited northeast of the volcano by tropospheric and stratospheric transport (Varekamp et al., 1984). In addition, ash particles and volatiles, specifically sulfurous species, formed a concentrated aerosol cloud in the stratosphere that was detectable for 21 days (Matson, 1984). Prior to the 1982 eruption, little was known about the volcano, but because the eruption affected many lives, caused severe casualties (approximately 2000 deaths; De la Cruz-Reyna and Martin Del Pozzo, 2009), and produced local and global environmental impacts, El Chichón has garnered a reputation as an extremely hazardous volcano, and has become the focus of intense study (Annen and Wagner, 2003; Scolamacchia and Capra, 2015, and references therein).

The 1982 El Chichón eruption has been recognized as an example where compositionally and isotopically evolved magma resides in the shallow crust, and reactivates prior to eruption due to recharge with more primitive magma (e.g., Davidson and Tepley, 1997; Tepley et al., 2000; Davidson et al., 2001; Andrews et al., 2008). Zoned plagioclase has systematically high $^{87}Sr/^{86}Sr$ in crystal interiors suggesting crustal assimilation during shallow magma storage, whereas rims are lower

* Corresponding author at: Institut für Geowissenschaften, Universität Heidelberg, Im Neuenheimer Feld 234-236, 69120 Heidelberg, Germany.
E-mail addresses: pack.brenda1012@gmail.com (B. Pack), axel.schmitt@geow.uni-heidelberg.de (A.K. Schmitt), robergejulie@gmail.com (J. Roberge), felizta@hotmail.com (F.G. Tenorio), damiata@ucla.edu (B.N. Damiata).

http://dx.doi.org/10.1016/j.jvolgeores.2016.01.011
0377-0273/

in $^{87}Sr/^{86}Sr$ indicative of recharge and mixing with more primitive magma (Davidson and Tepley, 1997; Tepley et al., 2000; Davidson et al., 2001; Andrews et al., 2008). Interaction between deep and shallow magma reservoirs is also supported by trends in seismicity during the eruption: seismic foci migrated downwards (from ~2 km to ~15 km) indicating a transition from events directly associated with migration of magma and magma–groundwater interaction at shallow depth to regional tectonic strain in the wake of the eruption (Havskov et al., 1983). Despite this evidence for shallow magma storage, recharge, mixing and hybridization, the timescales and processes of magma residence at shallow levels remain poorly constrained for El Chichón. Eruptive recurrence intervals at El Chichón are brief (100–600 year; Tilling et al., 1984), and timescales of crystallization of major minerals are within a few 1000's years based on a ca. 1.3 ka U–Th isochron for groundmass and plagioclase, hornblende, augite, titanomagnetite, and anhydride (Pickett et al., 1993). Despite the longevity of volcanism at El Chichón (dating back to ca. 372 ka based on $^{40}Ar/^{39}Ar$ ages for accidental lithics; Layer et al., 2009), the 1982 eruption therefore appears to have tapped magma which shared little to none crystal heritage with its precursors, and was stored only briefly in an ephemeral magma reservoir (Tepley et al., 2000).

Zircon, a ubiquitous accessory mineral found in intermediate and evolved magmatic rocks, can be used to date crystallization in evolved melts (e.g., Schmitt, 2011). Because of zircon's low solubility in such melts and its extreme retentivity for geochronologically important elements, it distinctively can trace crustal assimilation and crystal recycling (e.g., Watson, 1996). Zircon also exerts significant control over the chemical properties of magmas. Multiple detailed petrographic studies have been carried out on 1982 and older El Chichón rocks (e.g., Juvigné, 1983; Luhr et al., 1984; Rose et al., 1984; Macías et al., 2003; Arce et al., 2014, 2015). None of these studies mentioned zircon, seemingly precluding the use of zircon as a quantitative indicator for crystal storage in the subvolcanic plumbing system of continental arc volcanoes (e.g., Bacon et al., 2000; Bacon and Lowenstern, 2005; Claiborne et al., 2010; Walker et al., 2010; Stelten and Cooper, 2012; Klemetti and Clynne, 2014; Schmitt et al., 2014). Here, we report the discovery of zircon crystals in heavy mineral separates from El Chichón rocks. Zircon crystals were investigated by electron beam imaging methods, including color cathodoluminescence (CCL) and distinct crystal domains visible in CCL were dated by U–Th and U–Pb methods. We demonstrate that interior domains indicate incomplete assimilation of crustal rocks, followed by overgrowth of zircon in a late Pleistocene to Holocene intrusive complex from which zircon was recycled prior to eruption.

2. Regional geological setting

El Chichón volcano, located in the Chiapas state of southern Mexico, comprises a trachyandesitic tuff cone and lava dome complex (Fig. 1). The volcano has been difficult to access in the past due to its remoteness, dense vegetation and rugged topography (Müllerried, 1932). It is the only active volcano in the Chiapanecan arc, and it is situated in an unusual location ~400 km from the Central American Trench and ~300 km above the subducted Cocos slab (Pardo and Suarez, 1995; Rebollar et al., 1999; García-Palomo et al., 2004). Competing scenarios for the origin of El Chichón magmatism are discussed in the literature: east-dipping subduction of the Cocos plate underneath the North American plate at the Central American Trench (Luhr et al., 1984, García-Palomo et al., 2004), devolatilization of the serpentinized Tehuantepec ridge (Manea and Manea, 2008), or extension and decompression melting, possibly with contributions of metasomatised mantle from former west-dipping subduction of the Yucatan plate (Kim et al., 2011; Arce et al., 2014).

Following the 1982 eruption, significant effort has been invested in establishing the chronostratigraphy of El Chichón. Here, we use the nomenclature of Espindola et al. (2000), which has been firmly established in the literature (e.g., Layer et al., 2009; Arce et al., 2014, 2015; Scolamacchia and Capra, 2015). The base unit O from Espindola et al. (2000) consists of porphyritic trachyandesitics rocks cropping out along the margins of a 2-km wide central collapse structure (Somma) which is concentric with the smaller 1982 crater. The Somma lavas were dated by K–Ar techniques to 209 ± 19 ka and 276 ± 6 ka (ages cited in Espindola et al., 2000), but Holocene lavas also exist along the Somma rim (Layer et al., 2009). Pre-Somma lavas (372 ± 5 ka) have thus far only been detected as accidental clasts (Layer et al., 2009). The oldest pyroclastic unit, N, comprises block and ash flow deposits which are locally overlain by Unit M, a porphyritic, andesitic lava flow rich in plagioclase and hornblende phenocrysts. Units L, K, and I consist of matrix-supported ash flow deposits with gravel-size andesitic clasts. Two distinctive deposits of surge and block-and-ash flow deposits make

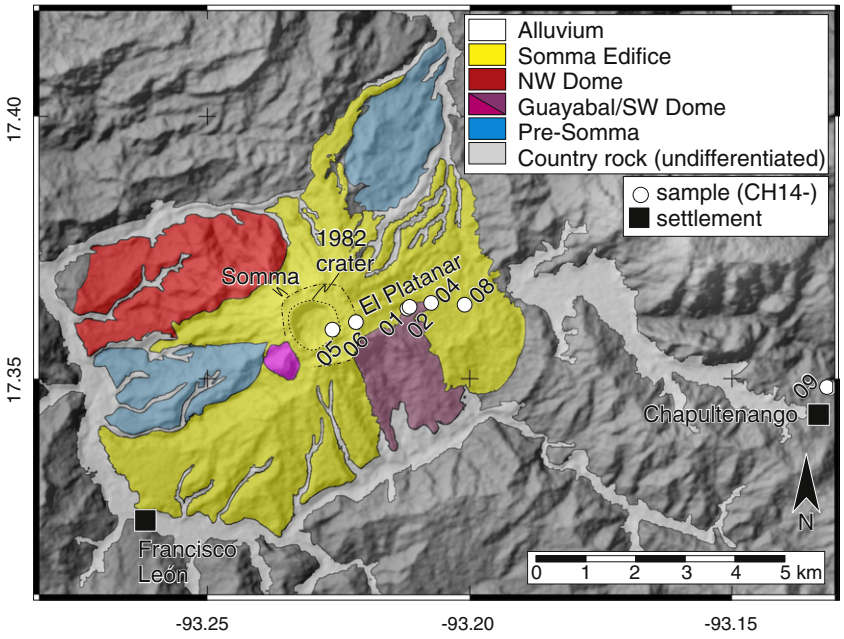

Fig. 1. Geologic sketch map showing major units of El Chichón volcano (after Layer et al., 2009) along with sampling locations from this study.

Table 1
AMS ^{14}C charcoal results with uncalibrated (for comparison with published values) and calibrated (for comparison with other timescales) ages. Locations see Table 2.

Sample	UCI AMS#	Type	$\delta^{13}C$ ‰	±	Modern fraction	±	$\Delta^{14}C$ ‰	±	^{14}C age (BP)	±	Calibrated Date cal AD*
CH14-01	144247	Charcoal	−25.7	0.1	0.821	0.0014	−179	1.4	1585	15	421–537 (95.4%)
CH14-02	144248	Charcoal	−25.8	0.1	0.9357	0.0016	−64.3	1.6	535	15	1330–1340 (4.6%) 1396–1431 (90.8%)

Radiocarbon concentrations are given as fractions of modern standard, $\Delta^{14}C$, and conventional radiocarbon age, following the conventions of Stuiver and Polach (1977). All results have been corrected for isotopic fractionation according to the conventions of Stuiver and Polach (1977), with $\delta^{13}C$ values measured on prepared graphite using the spectrometer. These values can differ from $\delta^{13}C$ of the original material if fractionation occurred during sample graphitization or the AMS measurement, and are not shown. The $\delta^{13}C$ values that are from Gas Bench aliquots measured to a precision of <0.1‰ relative to standards traceable to PDB (Craig, 1957), using a Thermo Finnigan Delta Plus stable-isotope mass spectrometer (IRMS)
* ages calculated as 95% highest probability range using Ox Cal v. 4.2.3.

up intercalated unit J where abundant carbonized logs have yielded an age of 3105 ± 70 BP (this and other ^{14}C ages cited from Espindola et al., 2000). Unit H, at approximately 2500 BP, is composed of six stratified beds rich in accretionary lapilli. Units G consists of surge beds, whereas the unit above, F, is an ash flow deposit found only on the western side of the crater. It is separated from Unit G by a paleosoil, dated at 1650–1790 BP, and its depositional age of 1600 BP is based on rounding of several ^{14}C ages for charred tree trunks. Unit E is a homogenous block and ash flow deposit (~4 m thick) with sand-sized matrix and gravel-to boulder-sized lithic clasts. In another location, Unit E directly overlies Unit I deposits, and branches from carbonized logs at different locations yielded overlapping radiocarbon ages of ~1500 BP. Unit D, from the base up, consists of silt-sized surge beds, followed by flow deposits with a total thickness of about 5 m. It is associated with archaeological artifacts (pottery, obsidian), and its rounded ^{14}C age is 1250 BP. Unit C has variable thickness, ranging from 1 to 15 m, and is composed of pumice flow deposits near the El Platanar gully and the area to the north of the crater. The paleosoil developed on top of Unit C yielded an age of 795 ± 50 BP and separates Unit C from Unit B, which can be identified as a characteristically yellow pumice fallout deposit where associated charcoal samples yielded radiocarbon ages from 550 to 700 BP. Outcrops of Unit B are poorly preserved, with most exposures to the southeast of the crater. Lastly, the youngest Unit A comprises the fallout overlain by pyroclastic flow and surge deposits from the 1982 eruption. The initial explosive phase destroyed the pre-existing lava dome, and the subsequent eruptions led to the formation of pyroclastic flows and surges extending as far as approximately 8 km from the vent. Young dome lavas are also exposed within the 1982 crater.

3. Materials and methods

Seven rock samples from El Chichón volcano were obtained for a reconnaissance study of zircon internal textures and ages (Fig. 1; Supplementary Fig. 1). Samples were selected based on the stratigraphy in Espindola et al. (2000), but two deposits in the El Platanar gorge were re-dated by ^{14}C methods using charcoal collected adjacent to the pumice used for zircon extraction (Table 1). We concentrated on the Holocene eruption phase, targeting the most recent (Units A and B) and some accessible older units (Units D and E, although the sample from Unit D was subsequently identified by ^{14}C dating as part of Unit E; Table 1). Pyroclastic deposits were sampled by collecting juvenile pumiceous materials from proximal pyroclastic flow deposits exposed in the El Platanar gorge (CH14-01, -02, -04, and -08), and a more distal (ca. 8 km from the vent) fall-out deposit near the village of Chapultenango (CH14-09). Two additional samples were from lavas; one from the bottom of the E wall of the 1982 crater (CH14-05), and one from the E Somma rim (CH14-06).

Samples (ca. 0.5 to 2 kg) were crushed, sieved into four fractions (<63 μm, 63–96 μm, 96–250 μm, >250 μm), washed with water to remove clay-sized grains, and rinsed with acetone to expedite drying. Individual size fractions were panned using a pristine commercial plastic pan for gold panning filled with water and a small amount of dish detergent to mechanically separate the heavy and light minerals. Zircon crystals ranging in size between 96 and 250 μm were further separated from the magnetic (which was extracted with a hand-magnet) and the light fractions (which floated after immersion in diiodomethane with a nominal density of 3.3 g/cm^3).

Twelve to fifteen individual grains from each sample were subsequently hand-picked and placed in rows onto double-coated polyimide tape glued flat onto an Al plate. In addition, AS3 zircon reference grains were added. A ~25 mm inner diameter teflon mold was placed on top of the tape with the zircon grains, and then filled with Buehler Epoxicure resin. After the epoxy was cured overnight, the mount was removed from the mold and its back lathed to a thickness of ~5 mm. The mount was then polished using 1200 grit SiC paper and 1 μm water-based

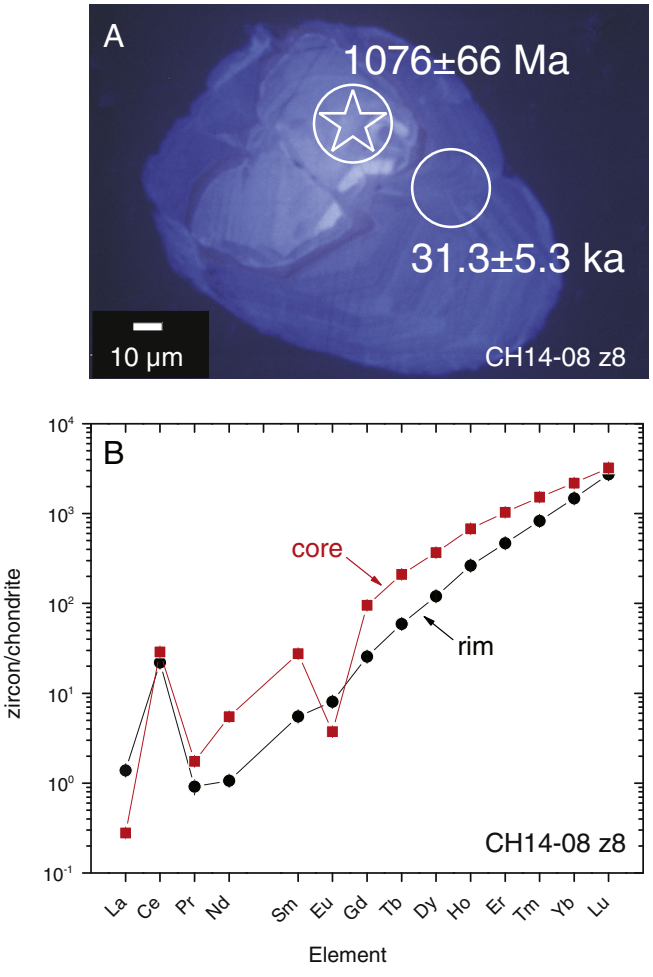

Fig. 2. Color cathodoluminescence (CCL) image for zircon CH14-08 z8 acquired with a TESCAN Vega XMU scanning electron microscope (SEM) and a rainbow CL detector. Zircon grain was selected from the 96 to 250 μm size fraction. Rim and core analysis locations are indicated together with U–Th and U–Pb SIMS ages, respectively. The spot with a star indicates that the core ages is in $^{230}Th/^{238}U$ secular equilibrium. Corresponding rare earth element (REE) data for zircon CH14-08 z8 rim and core following grinding and re-polishing after geochronological analysis.

Table 2
SIMS U–Th zircon results.

Sample	Zircon	Spot	(^{238}U)/(^{232}Th)	±	(^{230}Th)/(^{232}Th)	±	m	±	age (ka)	+	−	U (ppm)	Remarks
CH14-05 Lava sample from an autobrecciated dome within the crater of El Chichon (N 17.35935,E −93.2261, 724 m)													
CH14-05	1	Core	9.99	0.19	3.09	0.65	0.233	0.072	29.1	10.8	−9.8	305	
CH14-05	1	Rim	6.84	0.12	2.86	0.45	0.320	0.077	42.2	13.1	−11.7	302	
CH14-05	2	Interior	9.89	0.17	3.19	0.39	0.247	0.044	30.9	6.7	−6.3	818	
CH14-05	3	Interior	6.97	0.25	6.78	0.58	0.969	0.106	380	∞	−162	376	Core overlap
CH14-05	4	Core	9.71	0.17	9.73	0.54	1.00	0.07	∞	∞	∞	714	U–Pb age
CH14-05	4	Rim	9.51	0.16	4.50	0.33	0.412	0.040	57.8	7.7	−7.2	868	
CH14-05	5	Interior	5.64	0.10	2.26	0.32	0.273	0.069	34.9	10.9	−9.90	396	
CH14-05	6	Interior	4.99	0.08	2.12	0.17	0.282	0.043	36.4	7	−6.6	801	
CH14-05	7	Interior	7.24	0.12	4.34	0.37	0.536	0.060	84.1	15.5	−13.5	436	
CH14-05	9	Interior	5.53	0.10	2.25	0.24	0.277	0.053	35.6	8.5	−7.9	559	
CH14-05	10	Core	5.42	0.09	1.68	0.22	0.155	0.050	18.5	6.8	−6.4	503	
CH14-05	10	Rim	5.48	0.10	1.93	0.19	0.209	0.043	25.5	5.9	−5.6	955	
CH14-05	11	Rim	11.0	0.2	10.4	0.4	0.941	0.040	298	101	−51.6	1840	U–Pb age
CH14-05	11	Core	13.9	0.2	5.88	0.48	0.379	0.038	52.2	7.00	−6.50	681	
CH14-05	12	Core	10.6	0.18	10.4	0.4	0.980	0.050	422	∞	−131	1210	U–Pb age
CH14-05	12	Rim	12.7	0.2	4.73	0.50	0.319	0.043	41.9	7.1	−6.6	586	
CH14-05	13	Core	4.57	0.09	2.63	0.15	0.458	0.044	66.9	9.2	−8.5	1240	
CH14-05	13	Rim	10.9	0.2	5.02	0.24	0.407	0.025	56.8	4.8	−4.6	1720	
CH14-08 Composite pumice (10–20 cm in diameter) from pyroclastic flow deposit overlain by surge and fall-out deposits (N 17.36411, E −93.2009, 677 m)													
CH14-08	1	Interior	9.87	0.17	3.93	0.42	0.331	0.048	43.8	8.2	−7.6	431	
CH14-08	2	Rim	7.04	0.12	2.71	0.23	0.284	0.039	36.6	6.1	−5.8	719	
CH14-08	2	Core	2.17	0.04	2.41	0.18	1.21	0.17	∞	∞	∞	412	
CH14-08	3	Interior	10.1	0.2	3.06	0.34	0.227	0.038	28.3	5.5	−5.2	464	
CH14-08	4	Interior	6.68	0.12	2.61	0.21	0.285	0.038	36.4	6	−5.7	770	
CH14-08	5	Interior	5.48	0.11	1.77	0.28	0.173	0.063	20.7	8.5	−7.8	441	
CH14-08	6	Interior	7.50	0.13	3.05	0.23	0.316	0.036	41.6	6	−5.7	855	
CH14-08	7	Interior	8.01	0.14	3.99	0.26	0.427	0.038	60.9	7.6	−7.1	1100	
CH14-08	8	Core	9.51	0.17	10.3	0.7	1.09	0.09	∞	∞	∞	602	U–Pb age
CH14-08	8	Rim	8.59	0.19	2.89	0.27	0.250	0.036	31.3	5.4	−5.2	560	
CH14-08	10	Core	14.8	0.4	16.0	0.78	1.09	0.06	∞	∞	∞	551	U–Pb age
CH14-08	10	Rim	8.83	0.15	4.05	0.56	0.390	0.072	54.0	13.7	−12.2	325	
CH14-08	12	Core	7.61	0.18	8.17	0.59	1.09	0.09	∞	∞	∞	399	U–Pb age
CH14-08	12	Rim	15.0	0.3	15.0	1.8	1.00	0.13	734	∞	−511	345	Core overlap
CH14-08	13	Interior	4.22	0.07	1.26	0.07	0.083	0.022	9.3	2.7	−2.7	1990	
CH14-09 Composite yellow pumice clasts (max. 10 cm in diameter) from fall-out deposit (N 17.34828, E −93.1315, 583 m)													
CH14-09	1	Interior	6.34	0.11	2.47	0.2	0.276	0.038	35.2	5.9	−5.6	672	
CH14-09	2	Core	6.49	0.13	2.47	0.22	0.269	0.041	34.2	6.2	−5.8	593	
CH14-09	2	Rim	4.37	0.07	1.17	0.13	0.052	0.039	5.8	4.7	−4.5	709	
CH14-09	3	Interior	11.3	0.2	5.38	0.34	0.426	0.034	60.9	6.8	−6.4	929	
CH14-09	4	Interior	4.21	0.1	2.15	0.33	0.360	0.104	48.7	19.5	−16.6	297	
CH14-09	5	Core	8.84	0.18	11.4	1.1	1.33	0.14	∞	∞	∞	580	
CH14-09	5	Rim	6.90	0.13	2.42	0.18	0.242	0.031	30.3	4.7	−4.5	947	
CH14-09	6	Interior	3.37	0.06	1.29	0.08	0.125	0.034	14.8	4.4	−4.3	1510	
CH14-09	7	Interior	5.49	0.1	2.01	0.33	0.226	0.074	28.1	10.9	−9.90	427	
CH14-09	8	Interior	12.3	0.2	5.67	0.53	0.414	0.048	58.5	9.3	−8.6	659	
CH14-09	9	Core	9.71	0.16	4.12	0.33	0.359	0.039	48.5	6.8	−6.4	906	
CH14-09	9	Rim	13.9	0.3	5.62	0.44	0.359	0.035	48.3	6.1	−5.8	868	
CH14-09	10	Interior	6.39	0.15	5.52	0.78	0.840	0.147	200	268	−70.9	593	U–Pb age
CH14-09	11	Interior	7.72	0.13	2.89	0.21	0.282	0.032	36.2	4.9	−4.6	1010	
CH14-09	12	Interior	6.00	0.1	2.59	0.23	0.319	0.047	42.0	7.8	−7.3	702	
CH14-09	13	Interior	5.08	0.09	1.87	0.13	0.215	0.032	26.5	4.5	−4.4	1840	
CH14-09	14	Interior	5.38	0.09	1.46	0.14	0.107	0.032	12.3	3.9	−3.8	947	
CH14-01 Composite pumice (10–15 cm in diameter) from base of pyroclastic-flow deposit (N 17.36320, E −93.21140, 724 m)													
CH14-01	1	Rim	5.05	0.05	1.62	0.39	0.156	0.095	18.4	13.0	−11.6	506	
CH14-01	2	Rim	8.32	0.07	3.13	0.31	0.292	0.042	37.7	6.7	−6.3	2300	
CH14-01	3	Rim	13.1	0.13	5.66	0.34	0.387	0.029	53.3	5.2	−5.00	4280	
CH14-01	4	Core	8.95	0.09	5.23	0.63	0.532	0.079	82.9	20.3	−17.1	836	
CH14-01	4	Rim	6.74	0.06	2.12	0.36	0.196	0.063	23.8	8.9	−8.2	942	
CH14-01	5	Rim	7.04	0.07	1.01	0.22	0.002	0.036	0.2	4.03	−3.88	905	
CH14-01	6	Rim	6.85	0.06	1.86	0.28	0.147	0.047	17.4	6.2	−5.9	1020	
CH14-01	7	Rim	7.03	0.07	2.74	0.26	0.290	0.043	37.4	6.8	−6.4	1880	
CH14-01	8	Rim	10.3	0.1	3.20	0.37	0.238	0.040	29.7	5.9	−5.6	1660	
CH14-01	10	Rim	6.04	0.06	1.98	0.19	0.197	0.039	23.9	5.4	−5.1	2190	
CH14-01	11	Rim	4.72	0.04	1.71	0.31	0.193	0.082	23.4	11.7	−10.6	1400	
CH14-01	13	Rim	3.04	0.03	1.16	0.15	0.083	0.072	9.4	8.9	−8.2	2030	
CH14-01	14	Rim	11.3	0.1	3.46	0.37	0.240	0.036	30.0	5.3	−5.0	2040	
CH14-01	15	Rim	10.2	0.1	3.15	0.45	0.235	0.049	29.2	7.3	−6.8	1720	
CH14-01	15	Rim 2	12.8	0.12	3.60	0.56	0.220	0.047	27.2	6.8	−6.4	940	Opposite end

(continued on next page)

Table 2 (*continued*)

Sample	Zircon	Spot	(^{238}U)/(^{232}Th)	±	(^{230}Th)/(^{232}Th)	±	m	±	age (ka)	+	−	U (ppm)	Remarks
CH14-01	16	Rim	4.07	0.04	1.73	0.24	0.240	0.078	29.9	12.1	−10.9	1590	
CH14-02 Single pumice clast (40 cm in diameter) from clast-rich zone in pyroclastic flow deposit overlying CH14-01 (N 17.36352, E −93.21130, 724 m)													
CH14-02	1	Rim	2.60	0.02	1.16	0.1	0.104	0.063	11.9	7.9	−7.4	2490	
CH14-02	3	Rim	5.32	0.05	1.57	0.29	0.133	0.067	15.8	9.0	−8.3	646	
CH14-02	4	Rim	7.39	0.07	1.51	0.43	0.081	0.067	9.2	8.3	−7.7	713	
CH14-02	5	Core	11.7	0.1	4.74	0.37	0.349	0.035	46.9	6.0	−5.7	1930	
CH14-02	5	Rim	7.83	0.08	1.71	0.33	0.105	0.048	12.2	6.1	−5.7	1300	
CH14-02	6	Core	2.42	0.02	1.11	0.08	0.082	0.056	9.7	7.1	−6.6	4060	
CH14-02	7	Core	4.81	0.05	1.20	0.15	0.054	0.039	6.1	4.7	−4.5	1300	
CH14-02	9	Rim	4.15	0.04	1.10	0.14	0.034	0.044	3.7	5.3	−5.1	2660	
CH14-02	11	Rim	12.2	0.1	4.61	0.27	0.324	0.024	42.6	4.0	−3.9	5310	
CH14-02	12	Rim	8.67	0.08	2.45	0.22	0.190	0.029	23.0	3.9	−3.8	2890	
CH14-02	13	Rim	5.27	0.05	1.34	0.15	0.081	0.035	9.3	4.4	−4.2	1910	
CH14-02	14	Core	3.32	0.03	1.19	0.12	0.085	0.052	9.6	6.5	−6.2	3760	
CH14-02	17	Rim	6.71	0.06	2.16	0.28	0.204	0.049	24.9	6.9	−6.5	1300	
CH14-04 Composite pumice (10–15 cm in diameter) sample from pyroclastic flow deposit directly underlying 1982 deposit (N 17.36444, E −93.20723, 683 m)													
CH14-04	1	Core	5.49	0.05	1.93	0.23	0.208	0.052	25.4	7.4	−6.9	1550	
CH14-04	1	Rim	7.15	0.07	1.16	0.26	0.026	0.043	2.9	4.9	−4.7	552	
CH14-04	2	Core	6.43	0.06	1.53	0.22	0.100	0.040	11.4	5.00	−4.8	1300	
CH14-04	3	Core	7.44	0.07	2.91	0.20	0.298	0.031	38.5	5.00	−4.8	2950	
CH14-04	4	Core	6.49	0.06	1.32	0.27	0.060	0.050	6.8	5.9	−5.6	393	
CH14-04	5	Core	8.82	0.08	2.86	0.23	0.239	0.030	29.8	4.3	−4.2	2390	
CH14-04	6	Interior	5.69	0.06	3.00	0.31	0.427	0.066	60.7	13.3	−11.8	1410	
CH14-04	6	Rim	5.03	0.04	1.36	0.24	0.090	0.060	10.3	7.5	−7.0	765	
CH14-04	7	Rim	4.87	0.05	1.22	0.16	0.059	0.041	6.7	4.9	−4.7	1500	
CH14-04	8	Rim	3.94	0.05	1.69	0.24	0.238	0.080	29.7	12.2	−10.9	1030	
CH14-04	9	Core	4.98	0.05	1.09	0.39	0.026	0.097	2.8	11.5	−10.4	1200	
CH14-04	10	Core	7.05	0.07	2.05	0.31	0.174	0.051	20.9	7.0	−6.5	1090	
CH14-04	11	Core	7.12	0.07	2.65	0.36	0.271	0.058	34.4	9.1	−8.4	1650	
CH14-04	11	Rim	6.15	0.06	1.49	0.28	0.096	0.053	10.9	6.6	−6.3	526	
CH14-04	12	Core	5.29	0.05	1.48	0.23	0.114	0.053	13.2	6.7	−6.3	1980	
CH14-04	13	Rim	6.24	0.06	2.29	0.24	0.248	0.045	31.1	6.8	−6.4	1800	
CH14-04	14	Core	2.08	0.02	1.15	0.07	0.144	0.068	17.0	9.0	−8.4	3180	
CH14-06 Lava sample from the E Somma ridge (N 17.36076, E −93.22614, 1079 m)													
CH14-06	1	Core	11.4	0.11	3.00	0.62	0.193	0.060	23.4	8.4	−7.8	1050	
CH14-06	1	Rim	5.24	0.05	1.53	0.19	0.126	0.044	14.6	5.6	−5.3	889	
CH14-06	2	Rim	5.91	0.06	1.66	0.24	0.136	0.049	15.9	6.3	−6.00	940	
CH14-06	3	Rim	7.44	0.07	1.92	0.23	0.143	0.036	16.9	4.6	−4.4	1370	
CH14-06	3	Core	17.6	0.2	14.8	0.64	0.831	0.040	194	29	−23	1310	Core overlap ?
CH14-06	4	Rim	6.62	0.07	2.09	0.21	0.196	0.038	23.8	5.3	−5.000	1540	
CH14-06	5	Rim	3.24	0.03	1.26	0.15	0.117	0.067	13.5	8.6	−8.0	1940	
CH14-06	6	Core	3.03	0.03	2.30	1.07	0.641	0.526	112	∞	−98	224	Core overlap
CH14-06	6	Rim	5.83	0.06	1.89	0.19	0.186	0.040	22.4	5.5	−5.3	1990	
CH14-06	7	Rim	8.62	0.08	2.15	0.29	0.152	0.038	17.9	5.0	−4.8	1170	
CH14-06	8	Rim	5.57	0.05	1.89	0.20	0.195	0.044	23.7	6.1	−5.8	1570	
CH14-06	10	Rim	7.80	0.07	1.84	0.24	0.125	0.035	14.5	4.5	−4.3	1250	
CH14-06	11	Core	11.3	0.1	4.00	0.46	0.293	0.045	37.8	7.1	−6.7	1280	
CH14-06	11	Rim	6.81	0.06	2.38	0.22	0.239	0.039	29.9	5.7	−5.4	1930	
CH14-06	12	Core	2.78	0.06	2.81	0.24	1.02	0.14	∞	∞	∞	937	Core overlap ?
CH14-06	13	Rim	6.88	0.07	1.80	0.21	0.138	0.035	16.2	4.6	−4.4	1190	
CH14-06	14	Rim	7.20	0.07	2.23	0.26	0.200	0.042	24.3	5.9	−5.6	1490	

Analytical uncertainties 1σ.
m = zircon melt model isochron slope; (^{238}U)/(^{232}Th) = 0.999 ± 0.045 and (^{230}Th)/(^{232}Th) = 0.993 ± 0.004 from Pickett and Murell (1997).
∞ = secular equilibrium.
Decay constants used: λ_{232}: $4.9475 \cdot 10^{-11}$ a^{-1}; λ_{230}: $9.158 \cdot 10^{-6}$ a^{-1}; λ_{238}: $1.55125 \cdot 10^{-10}$ a^{-1}.
Secular equilibrium zircon reference AS3 (^{230}Th)/(^{232}U) = 0.987 ± 0.011 (MSWD = 1.1; n = 26).
U concentration from measured $^{238}UO^+/^{90}Zr_2O_4^+$ relative to 91500 zircon with 81.2 ppm U.
Sample coordinates in WGS84, elevation in m above sealevel.

micro-diamond solution. Color cathodoluminescence (CCL) images were acquired using a TESCAN Vega XMU scanning electron microscope (SEM) at the University of California Los Angeles (UCLA). CCL imaging was carried out on uncoated samples in environmental mode using a "rainbow" CL detector with a collection band-width from 350 to 850 nm subdivided into three channels (Fig. 2; Supplementary Figs. 2–8). After imaging the mounts, they were cleaned using an ultrasonic bath and detergent, immersed into ~1 N HCl, and rinsed with deionized H_2O and ultimately methanol. An approximately 20-30 nm thick Au-coating was applied to the dried mount.

U–Th isotope analyses (Table 2) were made using a CAMECA ims1270 ion microprobe at UCLA following analyses techniques described in Reid et al. (1997); Schmitt (2011) with the modification that multi-collection using three electron multipliers was applied. This allowed the simultaneous detection of mass/charge 244 (background), 246 ($^{230}ThO^+$) and $^{238}UO^+$, reducing the duty cycle of the analyses by ca. 30%. U–Th analysis of zircon interiors visible by pink vs. blue CCL activity indicated that these domains were in secular equilibrium (i.e., >380 ka, but otherwise with an undefined age). The same interior domains and others with similar CCL appearance were subsequently analyzed for their U–Pb isotopic ages (Table 3) using the CAMECA ims1270 ion microprobe at UCLA and methods described in Schmitt et al. (2003). A total of 22 xenocrystic cores were targeted to obtain U–Pb ages. All data were reduced using ZIPS v. 3.0.4. (developed at UCLA by C. Coath). U–Th model ages were calculated using whole rock compositions from Pickett and Murrell (1997). Because their analyses of four different El Chichón units are indistinguishable within uncertainty, the average and standard deviation of these analyses were used for the

Table 3
SIMS U–Pb zircon results. Bold ages indicate those used for comparison with detrital zircon analyses (Weber et al., 2009).

Sample	Zircon	Spot	Age $^{206}Pb/^{238}U$	±	Age $^{207}Pb/^{235}U$	±	Age $^{207}Pb/^{206}Pb$	±	% Radiogenic 206Pb	$^{206}Pb^*/^{238}U$	±	$^{207}Pb^*/^{235}U$	±	$^{207}Pb^*/^{206}Pb$	±	Correlation of concordia ellipses	U ppm	Th/ U	U O/U	Pb corr.
CH14-05	4	Core	841	20	883	17.3	**991**	**29**	99.6	0.139	0.003	1.39	0.04	0.0722	0.0010	0.88	217	0.36	8.79	(^{204}Pb)
CH14-05	11	Rim	65.5	2.0	76.57	8.27	**437**	**222**	98.2	0.0102	0.0003	0.0783	0.0088	0.0556	0.0056	0.51	281	0.25	8.75	(^{204}Pb)
CH14-05	12	Core	954	22	939	21	**903**	**50**	98.6	0.160	0.004	1.52	0.05	0.0691	0.0017	0.71	106	0.23	9.04	(^{204}Pb)
CH14-08	8	Core	599	13	709	21	**1076**	**66**	96.7	0.0974	0.0023	1.01	0.04	0.0753	0.0025	0.62	170	0.24	9.21	(^{204}Pb)
CH14-08	10	Core	**290**	**9**	287	27	264	216	96.4	0.0460	0.0015	0.327	0.035	0.0515	0.0048	0.53	76	0.65	8.46	(^{208}Pb)
CH14-08	12	Core	**962**	**25**	929	27	851	63	98.0	0.161	0.005	1.50	0.07	0.0674	0.0020	0.73	126	0.32	8.45	(^{204}Pb)
CH14-09	10	Core	**516**	**14**	501	26	433	121	98.7	0.0834	0.0023	0.638	0.042	0.0555	0.0030	0.60	95	0.60	9.12	(^{204}Pb)
CH14-06	4	Core	**315**	**6**	335	11	474	97	100	0.0502	0.0011	0.391	0.015	0.0566	0.0025	-0.06	395	0.33	6.72	(^{204}Pb)
CH14-06	7	Core	**460**	**9**	449	17	391	94	99.6	0.0740	0.0015	0.556	0.026	0.0545	0.0023	0.46	617	0.32	6.78	(^{204}Pb)
CH14-06	9	Core	**466**	**16**	487	22	585	89	99.4	0.0750	0.0027	0.615	0.035	0.0595	0.0024	0.70	678	0.26	6.50	(^{204}Pb)
CH14-06	13	Core	**324**	**8**	258	45	b.d.	b.d.	98.0	0.0515	0.0013	0.289	0.057	0.0408	0.0075	0.53	251	1.23	6.58	(^{204}Pb)
CH14-06	14	Core	126	3	150	7	**552**	**116**	99.5	0.0197	0.0004	0.159	0.008	0.0586	0.0031	0.19	1226	0.26	6.89	(^{204}Pb)
CH14-04	6	Core	269	6	354	19	**962**	**110**	99.5	0.0426	0.0009	0.418	0.027	0.0712	0.0038	0.60	722	0.60	6.41	(^{204}Pb)
CH14-02	1	Core	**437**	**9**	412	22	276	138	98.6	0.0701	0.0015	0.500	0.032	0.0518	0.0031	0.31	748	0.45	6.83	(^{204}Pb)
CH14-02	8	Core	72.2	1.6	111	5	**1051**	**79**	99.9	0.0113	0.0002	0.116	0.005	0.0744	0.0029	0.47	1224	0.33	7.08	(^{204}Pb)
CH14-02	15	Core	1492	55	1666	38	**1894**	**37**	100	0.260	0.011	4.16	0.20	0.116	0.002	0.90	184	1.55	6.78	(^{204}Pb)
CH14-02	16	Core	956	38	973	41	**1012**	**104**	99.7	0.160	0.007	1.61	0.11	0.0729	0.0037	0.63	106	0.38	6.84	(^{204}Pb)
CH14-01	4	Core	1266	39	1399	33	**1608**	**38**	99.5	0.217	0.007	2.97	0.13	0.0991	0.0020	0.88	248	0.17	6.78	(^{204}Pb)
CH14-01	8	Core	**598**	**24**	595	38	586	145	99.7	0.0971	0.0041	0.797	0.068	0.0595	0.0040	0.63	124	0.73	6.84	(^{204}Pb)
CH14-01	11	Core	1335	42	1478	40	**1690**	**72**	98.9	0.230	0.008	3.29	0.17	0.104	0.004	0.65	135	0.95	7.03	(^{204}Pb)
CH14-01	13	Core	**382**	**12**	385	32	404	213	99.4	0.0611	0.0020	0.461	0.045	0.0548	0.0052	0.26	193	1.06	6.75	(^{204}Pb)
CH14-01	15	Core	**352**	**11**	314	59	39	500	98.4	0.0561	0.0018	0.362	0.080	0.0468	0.0098	0.40	104	0.60	6.74	(^{204}Pb)

Analytical uncertainties 1σ.
Decay constants used: λ_{232}: $4.9475 \cdot 10^{-11}$ a^{-1}; λ_{238}: $1.55125 \cdot 10^{-10}$ a^{-1}.
Common Pb correction: $^{206}Pb/^{204}Pb = 18.86$, $^{207}Pb/^{204}Pb = 15.62$, $^{208}Pb/^{204}Pb = 38.43$.
UO^+/U^+ vs. Pb^+/U^+ calibration slope = 0.5–9.53 ± 0.18; external reproducibility of AS3 $^{206}Pb/^{238}U$ age = 1.8% (n = 5; Aug 2014); 1.15–3.37 ± 0.04; external reproducibility of AS3 $^{206}Pb/^{238}U$ age = 1.1% (n = 8; Jan 2015).
Th^+/U^+ relative sensitivity 0.957 (Aug 2014) and 1.01 (Jan 2015).
U ppm from U/Zr_2O_2 (Aug 2014) and $U/^{94}Zr_2O$ (Jan 2015) relative to 91500 zircon with 81.2 ppm U.
Bold indicates preferred age.

melt composition. No significant difference exists between U/Th in El Chichón glass and whole rock (~0.3; Luhr et al., 1984), further supporting the choice of the whole rock average as representative for the melt.

Charcoal samples CH14-01 and CH14-02 were pretreated at the Keck Carbon Cycle accelerator mass spectrometry (AMS) facility, University of California, Irvine. The procedure to convert raw samples into graphite targets for AMS dating involved removal of macroscopic contaminants, chemical cleaning, combustion and graphitization. The samples were subjected to an Acid-Base-Acid (ABA) chemical cleaning to remove humic and fulvic acids (Olsson, 1986). The procedure involved application of approximately 6 mL of 1 N HCl for 30 min, followed by 1 N NaOH for at least 30 min and then 1 N HCl for another 30 min, all at temperatures between 70 and 90 °C. The samples were then neutralized with deionized water. Intermediate application of the base solution was repeated until a clear or slightly tan liquid appeared. Samples CH14-01 and CH14-02 required 15 and 20 rinses, respectively, indicating that they contained moderate to high amounts of humic and fulvic acids (i.e., either as part of the original sample or acquired post-depositionally). Incomplete removal of humic and fulvic acids during the pretreatment process could result in bias towards a more recent age. Approximately 2 mg of dried sample was then placed in a quartz tube along with cupric oxide to provide an oxygen source, plus silver wire to "getter" any impurities that may adversely impact the graphitization process. The tubes were sealed under vacuum using a gas torch and then combusted at 900 °C for 3 h to generate CO_2 gas. The tubes were then placed on a vacuum line and the gaseous samples were cryogenically moved to vials containing an iron-powder catalyst. The gaseous samples were converted into graphite via the hydrogen-reduction method by heating to 500 °C for 3 h. The graphite was then packed into aluminum sample pellets and analyzed by the AMS spectrometer. In addition, aliquots of the gaseous samples were collected from the vacuum line and analyzed separately for carbon stable isotopes using a Fisons NA-1500NC elemental analyzer equipped with a Delta-Plus IRMS stable-isotope mass spectrometer.

4. Results

4.1. ^{14}C charcoal

Samples CH14-01 and CH14-02 yielded stratigraphically consistent ^{14}C charcoal ages of 1585 ± 15 BP and 535 ± 15 BP. Calibrated ages are stated in Table 1, but for stratigraphic correlation we only use the uncalibrated ^{14}C age BP as was done in previous studies (Espindola et al., 2000). Based on our AMS ^{14}C results, we assign sample CH14-02 to the penultimate eruption of El Chichón (Unit B at 550 BP; Espindola

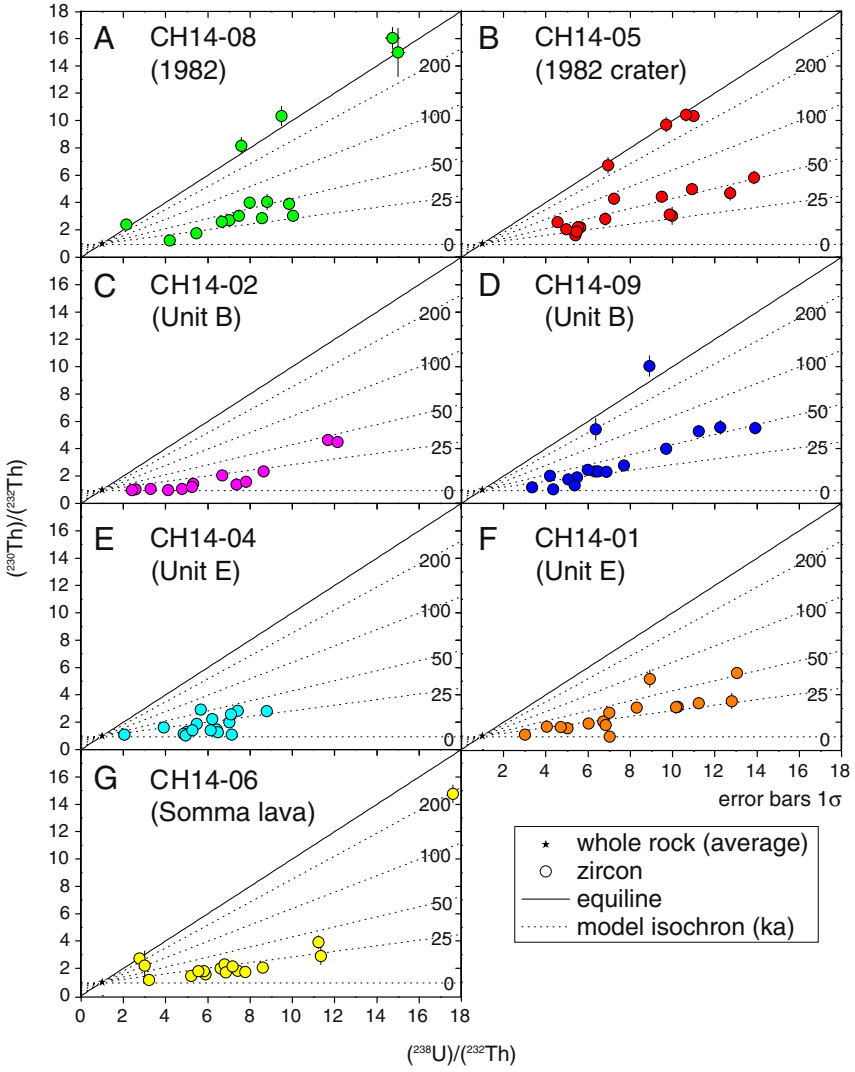

Fig. 3. U–Th isochron diagrams distributions for El Chichón samples. Zircon model ages were determined using the isochron slopes defined by zircon (from ion probe analysis using the CAMECA ims 1270 ion microprobe at UCLA) and whole rock (from published data) pairs. Analyses in secular equilibrium are those that overlap the equiline within 2σ uncertainties; corresponding U–Pb analyses are shown in Fig. 5.

et al., 2000). CH14-02 is thus a proximal equivalent to the yellow pumice fall-out from the 550 BP eruption (CH14-09). Although analytically consistent with published ^{14}C ages, there is disagreement between our new chronostratigraphic results and the stratigraphic sections published for the head of El Platanar gorge where we collected our samples (section 97a and Fig. 8 in Espindola et al., 2000). According to these workers, Unit B should only be present as a thin (<0.5 m) layer, whereas our sampling location for CH14-02 near the present stream level should be in Unit C based on comparison with Espindola et al. (2000); their Fig. 8; cf. Supplementary Fig. 1. Instead it yielded a younger age implicating it as belonging to Unit B. The location where CH14-01 was collected (Supplementary Fig. 1) has been mapped as Unit D with a rounded age of 1250 BP, but our age is more similar to the rounded 1600 BP age for Unit F (Espindola et al., 2000). Published ^{14}C ages for units E and F, however, overlap, and we thus tentatively attribute CH14-01 to Unit E, which has been previously mapped in other sections of El Platanar gorge (Espindola et al., 2000). CH14-04 was not directly dated at the sampling location, but based on the published stratigraphy, we also assign it to Unit E. No ambiguities exist regarding the yellow pumice fall-out of Unit B (CH0409) and the 1982 deposit (Unit A; CH0408) which cap all other units.

4.2. U–Th and U–Pb zircon geochronology

Electron beam imaging of polished zircon interiors often revealed zonation with interior domains that are pink in CCL images, contrasting with more blueish CCL colors for the rims (Fig. 2). The presence of these zonations guided placement of SIMS analysis spots and (after the exclusively xenocrystic nature of the pink cores was recognized) the choice of U–Th vs. U–Pb dating methods (Supplementary Figs. 2–8). We also performed reconnaissance rare earth element (REE) analyses on a single representative crystal (Fig. 2). The data indicate higher abundances for the mid REE (by a factor of ~6 for Sm) for the pink xenocrystic zircon interiors compared to the blue late Pleistocene rims (Fig. 2). The exception is Eu, which shows a stronger negative anomaly in the xenocrystic interior compared to the younger magmatic rim. More blueish CCL activity in REE-poorer zircons qualitatively agrees with findings in Belousova et al. (1998).

U–Th zircon data for all Holocene Chichón samples populate a widespread range in isotopic compositions in the U–Th isochron diagram (Fig. 3). Model isochrons are based on the average of four whole rock compositions for El Chichón reported by Pickett and Murrell (1997) as the anchoring point. El Chichón U–Th whole rock compositions show minor variability, which is propagated (as 1 standard deviation) into the uncertainties for the U–Th zircon model ages. The consistency of many near-zero model ages with a Holocene eruption age also supports the choice of the average U–Th whole rock composition.

For the 1982 lava sample (CH14-05), the youngest zircon age is 18.5 + 6.8 / −6.4 ka while the oldest is 84.1 + 15.5 / −13.5 ka (Table 2). There are additional analyses with measurement uncertainties overlapping secular equilibrium, such as grain 12 with an apparent age of 422 + ∞ / −131 ka (secular equilibrium indicated by the infinity symbol ∞; Table 2). The same crystal has a significantly younger rim (41.9 + 7.1 / −6.6 ka; Fig. 3), and the interior was subsequently dated by U–Pb and identified as xenocrystic (Fig. 4). The apparent age of 422 + ∞ / −131 ka is thus geologically not meaningful, and it reflects secular equilibrium (within analytical error). Similar observations hold for the other samples. The pumice sample from the 1982 eruption, CH14-08, has ages ranging from 9.3 ± 2.7 ka to 60.9 + 7.6 / −7.1 ka (Table 2). Again, there are several analyses that are indistinguishable from secular equilibrium within uncertainty which were confirmed as xenocrystic (Fig. 4). Zircon ages for sample CH14-02 (identified as the 550 BP Unit B) range between 3.7 + 5.3 / −5.1 ka and 46.9 + 6.0 / −5.7 ka. This is similar to the stratigraphically equivalent sample CH14-09 (yellow pumice from the Unit B distal fall-out deposit) where ages range between 5.8 + 4.7 / −4.5 ka and 60.9 + 6.8 / −6.4 ka

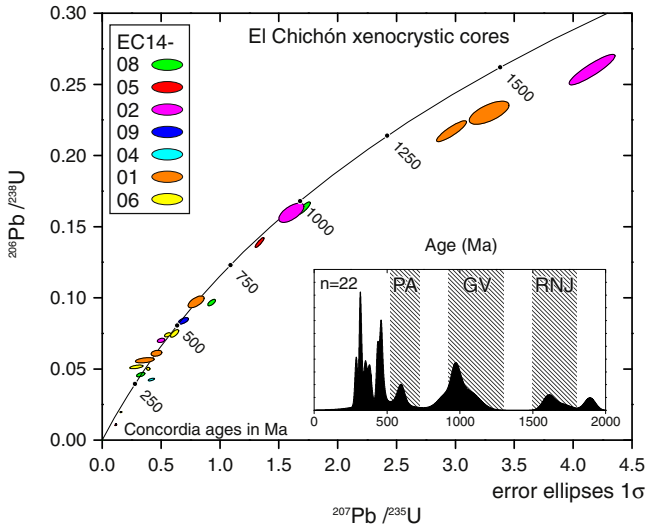

Fig. 4. U–Pb zircon results for El Chichón samples. Analyses were made using the CAMECA ims1270 ion microprobe at UCLA. Xenocrystic domains are interpreted as evidence for crustal contamination of El Chichón magmas assimilating buried basement rocks or sediments. Inset plot shows xenocryst ages in comparison to major regional crust-forming episodes PA (Pan African), GV (Grenville), and RNJ (Rio Negro-Juruena) after Weber et al. (2009).

(excluding analyses that are analytically indistinguishable from secular equilibrium). CH14-04 is from a pyroclastic flow unit (Unit E; nominal ^{14}C age 1500 BP; Espindola et al., 2000) which directly underlies the 1982 deposit. Zircon crystals from CH14-04 yielded U–Th ages that range from 2.8 + 11.5 / −10.4 ka to 60.7 + 13.3 / −11.8 ka. On average, younger crystals are more abundant in CH14-04 compared to the overlying deposit, although in both cases zircon crystals are much older than the eruptions ages. Sample CH14-01 (Unit E), which underlies CH14-02 (Unit B), has zircon ages ranging from 0.2 + 4.0 / −3.9 ka to 82.9 + 20.3 / −17.1 ka. Somma lava (CH14-06) has an unknown eruption age, but based on zircon ages between 13.5 + 8.6 / −8.0 ka and 37.8 + 7.1 / −6.7 ka it is clearly younger than Somma lavas dated to 209 ± 19 ka and 276 ± 6 ka (Espindola et al., 2000). Few older core analyses are suspect because of overlap onto xenocrystic cores in secular equilibrium (e.g., CH14-06 z6).

Secular equilibrium spots determined from U–Th geochronology, as well as conspicuously pink interiors were analyzed by U–Pb methods. These yielded ages between ca. 290 Ma and 1.9 Ga (Fig. 4). On a concordia diagram, most data plot near concordia showing only minor discordance. Only the oldest zircons fall on a discordia with a lower intercept of ca. 900 Ma, whereas three discordant analyses with younger (<290 Ma) apparent ages tend towards the origin, suggesting either very recent Pb loss, or, more likely based on post-analysis imaging of the SIMS spot locations, lateral beam overlap between interior and rim domains. Because of this, they are excluded from further discussion.

5. Discussion

5.1. Zircon in continental arc volcanoes

Zircon is known to be a reliable magma chronometer due to its sluggish diffusion rate for uranium and its intermediate daughters (Cherniak et al., 1997). Furthermore, it is able to record magma differentiation because it will only crystallize in comparatively evolved (and Zr-enriched) magmas whereas hot, mafic magma will rapidly dissolve zircon (e.g., Watson, 1996; Boehnke et al., 2013). The presence of zircon predating the eruption, either as “antecrysts” which are derived from coeval plutons in the subvolcanic environment or as “xenocrysts” from the country rock, can thus be expected in evolved magmas, whereas melts that are strongly undersaturated in zircon can completely resorb

preexisting zircon within several 100 years (e.g., Bacon and Lowenstern, 2005). Although dissolution timescales are rapid in undersaturated melts, antecrystic zircon, often predating the eruption by many 10's to 100's of ka, typically dominates over zircon with near-eruption ages in arc magmas, and these crystals are interpreted to be recycled from a largely crystalline subvolcanic magma reservoir or plutonic complex (e.g., Crater Lake: Bacon et al., 2000; Bacon and Lowenstern, 2005; Mount St. Helens: Claiborne et al., 2010; Aucanquilcha: Walker et al., 2010; South Sisters: Stelten and Cooper, 2012; Mount Lassen: Klemetti and Clynne, 2014; Hasan Dağı: Schmitt et al., 2014). Remarkably, xenocrystic zircon is rare in most continental arc volcanoes (see previous references; cf. Garrison et al., 2006) despite geochemical evidence that mantle derived magmas in these environments are inevitably crustally contaminated. The lack of xenocrystic zircon reflects that crustal assimilation is most efficient at high temperatures where zircon of country-rock provenance becomes rapidly resorbed. In this context of previous studies of zircon in continental arc volcanic rocks, two major differences emerge for El Chichón: (1) antecrystic zircon is abundant, but ages do not extend past ca. 84 ka; zircon thus lacks any evidence for recycling from the mid Pleistocene precursors of modern El Chichón, and (2) xenocrystic domains are present in a significant (~30%) proportion of the zircon population. The implications of these observations regarding zircon provenance in Holocene El Chichón rocks are discussed below.

5.2. Zircon and the timing of El Chichón magmatism

The presence of zircon in El Chichón rocks can uniquely constrain the age of the intrusive system underneath the volcano, and shed new light on the origins of evolved magma that blended into, and erupted with more mafic magma recharge (Davidson and Tepley, 1997; Tepley et al., 2000; Davidson et al., 2001; Macías et al., 2003; Andrews et al., 2008). Although the number of U–Th analyses per sample (n = 10–16) is too restricted to provide firm constraints on similarities and differences between individual samples, the overall ranges and major peaks in the U–Th age distribution (e.g., at ca. 10 ka and 30–40 ka) are common to all samples (Fig. 5). With the caveat that sampling density is low, Kolmogorov–Smirnov statistics applied to zircon ages (Fletcher et al., 2007) confirms that the U–Th dated domains are mostly statistically indistinguishable between individual samples. The only exceptions

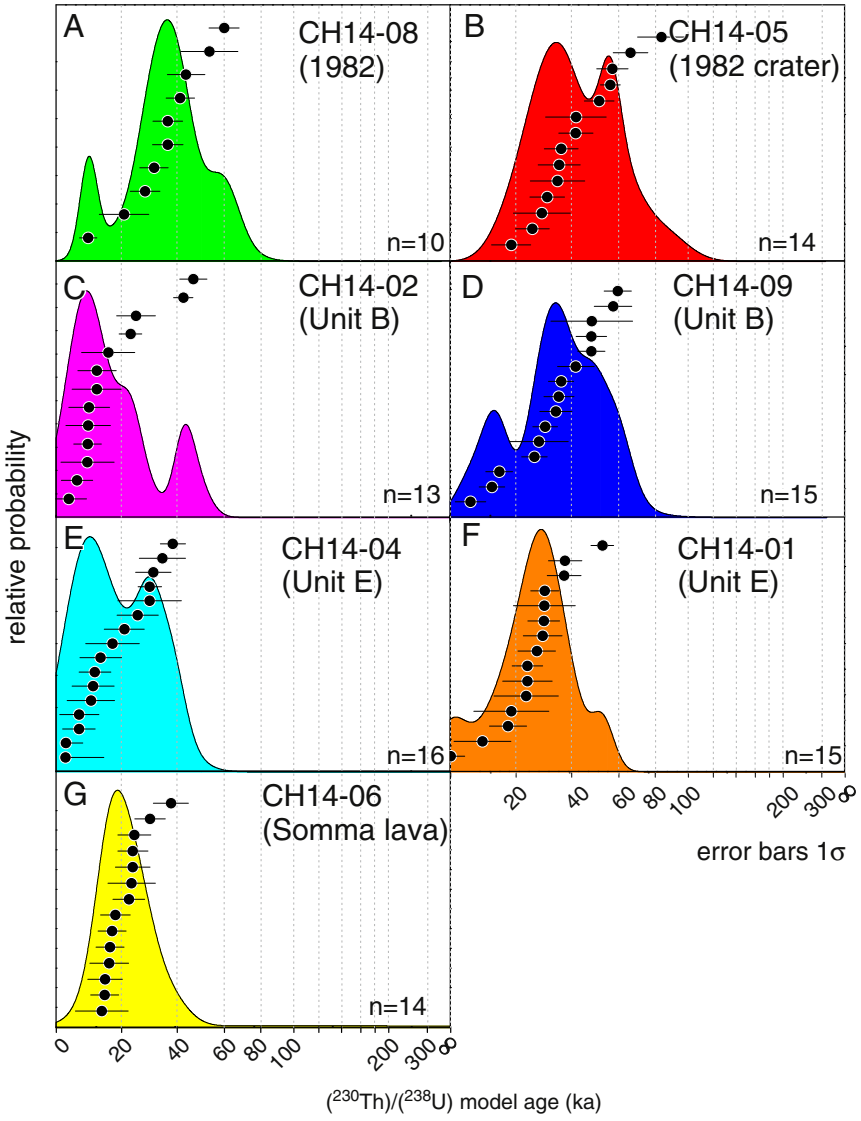

Fig. 5. Probability–density diagrams of U–Th model ages for El Chichón samples. Age distributions are consistent with continuous or frequent pulses of zircon crystallization dating back from near-eruption ages to ca. 84 ka. Several samples display common age peaks which suggest major magmatic pulses which predate the established stratigraphic record of the volcano. Note that age axis scaling is linear in relation to the (^{230}Th)/(^{238}U) activity ratio to better resolve younger ages, whereas older ages are compressed towards the right end of the plot. Data suspected of overlap onto secular equilibrium cores are omitted.

are the lava samples CH14-05 (1982 crater) and CH14-06 (Somma lava) which are dissimilar (with a probability $P < 0.05$ which is the limit to reject the null hypothesis for two populations being identical), and in the case of CH14-05 also distinct from CH14-02 (proximal 550 BP Unit B).

From comparing the age of zircon crystallization with the time of eruption, it is obvious that the duration of magma presence under El Chichón was much more long-lived than the period of frequent eruptions documented for the mid to late Holocene (Espindola et al., 2000). The zircon age distributions ranging back to ca. 84 ka prior to eruption overlap with $^{40}Ar/^{39}Ar$ ages for accidental lithics and peripheral lava domes to the NW and SW of the Holocene edifice (Layer et al., 2009). Our zircon results also confirm previous $^{40}Ar/^{39}Ar$ results (Layer et al., 2009; cf. Damon and Montesinos, 1978; Duffield et al., 1984), and indicate that Somma lavas are in part younger than ca. 20 ka. Older $^{40}Ar/^{39}Ar$ ages (up to 372 ± 5 ka; Layer et al., 2009), however, are not represented in the zircon age population (Fig. 6).

Collectively, the homogeneity of zircon ages suggests that all sampled units with eruption ages between ca. 1600 BP (Table 1) and 1982 tapped the same magma system containing zircons that have crystallized over several 10's of ka. The youngest crystals have ages that are analytically indistinguishable from the eruption age, but we emphasize that because zircon crystals were analyzed in cross-sections through crystal interiors, the outermost crystal rims could not be analyzed without contribution from older zircon mantles. This means that the youngest ages reported here are likely upper limits for the youngest phase of zircon crystallization. Absence of zircon from the Pleistocene (>84 ka) activity of El Chichón's precursors (e.g., the older part of the Somma volcano) is intriguing. With the caveat that some mixing between zircon domains of different age is possible, we argue that the lack of antecrystic zircon significantly older than ca. 84 ka is robust because sectioning will preferentially expose early formed zircon interiors at the surface (e.g., Samperton et al., 2015). The reasons for the absence of older antecrysts remain speculative because we only concentrated on the Holocene eruption phase, and it remains to be demonstrated if zircon is present in Pleistocene El Chichón rocks. Moreover, published eruption ages are based on K–Ar and Ar–Ar measurements with the possibility that unsupported ^{40}Ar could lead to overestimation of the eruption ages.

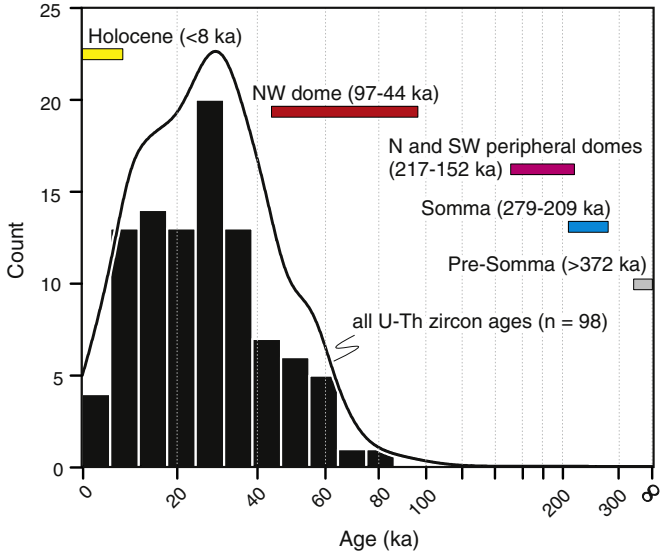

Fig. 6. Summary diagram of all U–Th model ages for El Chichón samples as histogram and probability–density curve in comparison with stages of the Pre-Holocene and Holocene evolution of El Chichón (according to published and unpublished ^{14}C and $^{40}Ar/^{39}Ar$ ages summarized in Scolamacchia and Capra, 2015). See comment on non-linear age axis in Fig. 5.

5.3. Zircon xenocrysts: provenance and resorption

Zircon xenocryst survival from assimilated country rocks is ubiquitous in Holocene El Chichón magmas. Xenocrysts are often identified as distinct CCL pink domains with rounded boundaries against CCL blue domains, and truncated interior oscillatory zonation. Where analyzed, these cores were found to be in secular equilibrium for (^{230}Th)/(^{238}U), in contrast to CCL blue overgrowths which show disequilibrium. U–Pb dating of these secular equilibrium domains yielded ages that predate the El Chichón magma system (Fig. 6). The presence of xenocrystic domains is consistent with isotopic disequilibrium in El Chichón magmas which is also evident from isotopically zoned plagioclase where high $^{87}Sr/^{86}Sr$ cores are overgrown by low $^{87}Sr/^{86}Sr$ rims (Davidson and Tepley, 1997; Tepley et al., 2000; Davidson et al., 2001; Andrews et al., 2008). Zircon xenocrystic cores can provide additional constraints on the nature of the crustal contaminant involved: their age distribution closely matches those of metasedimentary and metaigneous crystalline rocks of the Chiapas Massif Complex (Weber et al., 2008, 2009). One possible explanation for the provenance of xenocrystic zircons is thus that sediments underlying El Chichón carry zircons derived from basement in the highlands to the SW. This interpretation is supported by the mix of ages in the zircon cores which suggests that the assimilated source rocks already contained mixed zircon populations. These interpretations are tentative, because of the comparatively small number of zircon xenocrysts ($n = 22$) used in this comparison; more robust statistics would be required to place these conclusions on a firm foundation.

Zircon saturation temperatures (using the calibration of Boehnke et al., 2013 and published whole rock data from Luhr et al., 1984; Varekamp et al., 1984; Rose et al., 1984; Espindola et al., 2000; Macías et al., 2003; Layer et al., 2009; Arce et al., 2014) fall well below the ~800 °C eruption temperature estimated for El Chichón trachyandesites (e.g., zircon saturation temperatures are ~600 °C for 1982 pumice with Zr = ~140 ppm; Luhr, 1990; Luhr et al., 1984). This implies that the recharge magma was initially strongly zircon undersaturated and thus likely devoid of any zircon xenocrysts. However, at the time of eruption El Chichón magmas had elevated (~25–50 vol. %; e.g., Luhr et al., 1984; Varekamp et al., 1984) crystal contents, and the melt was consequently more enriched in Zr and had lower M values ($M = [Na + K + 2Ca] / [Al \times Si]$) compared to the bulk. Using the 1982 glass compositions (e.g., Luhr et al., 1984), we calculate Zr saturation concentrations of 365 ppm (at 800 °C) and 230 ppm (at 750 °C), compared to actual abundances of Zr = 200 ppm in the glass (inferred from glass Hf data in Luhr et al., 1984, and chondritic Zr/Hf = 38). Under these moderately to mildly zircon undersaturated conditions, a xenocryst of originally 100 μm would become resorbed to half its initial size over timescales of ~6×10^3 (800 °C) to ~1.2×10^5 (750 °C) years, according to the curves in Fig. 6 of Watson (1996). These timescales are maximum values that refer to the erupted trachydacite magma composition and temperature; for hotter magma recharge compositionally equivalent to rare mafic enclaves in El Chichón rocks (Zr ~100 ppm; Macías et al., 2003), undersaturation would be more severe, and resorption more rapid. Given that these timescales are commensurate to the overall duration of late Pleistocene–Holocene zircon crystallization for El Chichón, the survival of zircon xenocryst cores can only be explained if they mostly resided in near- or sub-solidus "cold-storage" (Cooper and Kent, 2014), rather than in a long-lived high-temperature magmatic environment.

According to zircon dissolution models (Watson, 1996), three factors that favor zircon xenocryst survivability are large crystal dimensions in the crustal assimilant, failure of the melt to coalesce into large magma bodies, and rapid (or weak) magmatic heating pulses. The size of zircon crystals in the El Chichón country rocks is unknown, but are unlikely to be larger than 100–200 μm typical for most detrital zircons. The arrested resorption of El Chichón xenocrysts thus suggests that assimilation occurred in small melt volumes (possibly via extraction of locally generated

anatectic melts) and fast, possibly via injection of small volumes of mafic to intermediate magma which cooled rapidly in a near-surface environment adjacent to cold country rock. Another factor that would aid zircon xenocryst survival is high Zr abundance in the assimilant. In fact, continental crustal averages (~200 ppm; Rudnick and Gao, 2004) are higher compared to mafic–intermediate magma recharge for El Chichón (~100–150 ppm; Luhr et al., 1984; Macías et al., 2003). It thus seems likely that initially undersaturated El Chichón trachydacite magma became saturated after it evolved through a combination of crustal assimilation and fractional crystallization.

5.4. Zircon constraints on magmatic processes at El Chichón

Zircon's durability and relative resistance to resorption is unlike any other magmatic crystal phase in El Chichón rocks. The internal zircon resorption and overgrowth textures are consistent with rapid thermal and/or compositional cycling, possibly in a series of recharge events. The oldest zircon crystals (barring xenocrystic cores) date back to ca. 84 ka (Fig. 6), which is younger than earlier magmatic events which formed the Pre-Somma, Somma, and peripheral domes (to the N and SW of the modern edifice; Layer et al., 2009; Scolamacchia and Capra, 2015). There is some overlap between zircon crystallization ages and eruption ages for the NW dome (Layer et al., 2009; Scolamacchia and Capra, 2015) but most zircon crystals postdate this episode of lateral dome formation (Fig. 6). Zircon U–Th ages extend down to Holocene ages, but show an apparent decline in the probability density distribution for ages <8 ka. We caution, however, that the most recent zircon crystallization might have gone undetected because of the positioning of the analysis spots onto sectioned zircon crystals where the outermost rims of the zircons cannot be sampled without overlap onto interior domains, and that the apparent underrepresentation of Holocene zircon rims could be due to this sampling bias. This comparative longevity of zircon is in stark contrast to major phases (plagioclase, amphibole, clinopyroxene) and magnetite which collectively lack evidence for protracted crystal residence based on their U–Th isochron age of 1.3 ± 2.3 ka (Pickett et al., 1993).

A frequent pattern of high $^{87}Sr/^{86}Sr$ (~0.706) plagioclase cores mantled by low $^{87}Sr/^{86}Sr$ (~0.704) in El Chichón rocks indicates intrusion of less contaminated mafic magma into a more contaminated reservoir, or reaction of recharge magma with a crustally contaminated boundary layer (Davidson and Tepley, 1997; Tepley et al., 2000; Davidson et al., 2001; Andrews et al., 2008). The compositional homogeneity of the erupted trachyandesites throughout El Chichón's phase of Holocene activity implies that the resulting hybrid magma reservoir was well mixed, despite isotopic heterogeneity in phenocrysts and the rare preservation of rounded mafic enclaves as witnesses for basaltic input into the system (e.g., Macías et al., 2003). Zircon adds a new aspect to this scenario in that it demonstrates that this boundary layer significantly

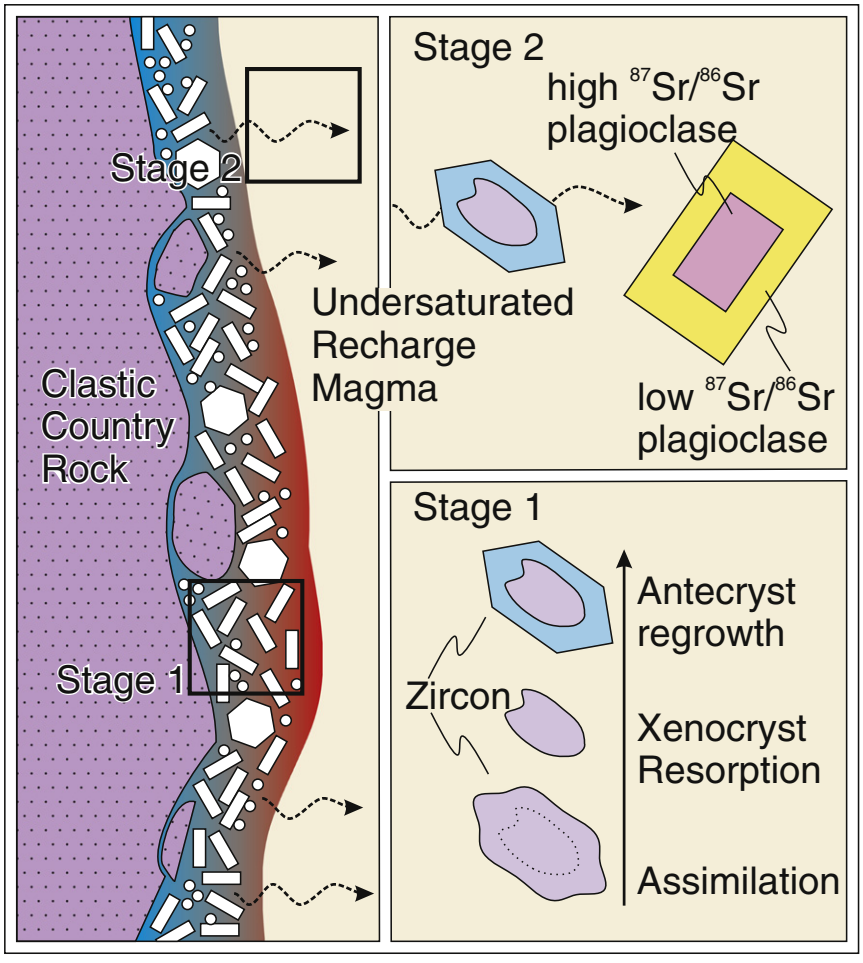

Fig. 7. Schematic of the Holocene magma reservoir and the pre-Holocene evolution of a crustally contaminated boundary layer from which xenocrystic zircon with antecrystic overgrowth are recycled. Stage 1 illustrates country rock assimilation, xenocrystic zircon resorption, and subsequent overgrowth once the magma reaches zircon saturation (between ca. 84 ka and near-eruption age). Stage 2 initiates with the extraction of high $^{87}Sr/^{86}Sr$ partial melt plus antecrystic zircon (sometimes with xenocrystic cores) from the contaminated boundary layer, followed by mixing with low $^{87}Sr/^{86}Sr$ recharge magma. During stage 2, plagioclase phenocrysts crystallized within few 100's to 1000's of years before the eruption and record the change in melt composition from more to less contaminated. Sketch is modified from Fig. 2 in Davidson et al. (2007); crystals are not to scale, and no specific geometry of the boundary layer is implicated.

predates the Holocene magma system, and that it selectively provided zircon (along with a chemical signal of elevated $^{87}Sr/^{86}Sr$) to the recharge magma (Fig. 7). Holocene eruptions then tapped this zircon reservoir which has not qualitatively changed despite multiple eruptions from 1600 BP onward, including the most recent event of 1982. Zircon xenocryst survival requires that crystals in this contaminated reservoir or boundary layer resided in a highly crystalline mush or subsolidus intrusions (e.g., Cooper and Kent, 2014) for most of their lifetime, with zircon assimilation, resorption and growth being restricted to brief episodes during ephemeral recharge and mixing events.

The absence of evidence for major phases being coeval with zircon (at least for the 1982 eruption; Pickett et al., 1993) is intriguing, and may hint at the special role that zircon plays in magmatic differentiation: its small crystal size makes it conducive to be transported with the melt (e.g., when melt extraction occurs at low degrees of partial melting), and by the same token it resists gravitational settling upon crystallization (Reid et al., 1997). Moreover, slow melt diffusion of Zr as its major stoichiometric component aids in its preservation under conditions where major phases may not survive. In this case, major phases (specifically: plagioclase) record only the chemical signal that resulted from magma recharge causing melts with high $^{87}Sr/^{86}Sr$ to become mobilized from a contaminated boundary zone between the eruptible interior of the magma reservoir and country rock, followed by progressive dilution with low $^{87}Sr/^{86}Sr$ magma as recharge and mixing progressed (Fig. 7). In contrast to zircon, carry-over of plagioclase from the boundary layer is dismissed based on young U–Th ages (Pickett et al., 1993), and the preservation of sharp transitions from high to low $^{87}Sr/^{86}Sr$ in plagioclase which are only permissive for brief (100's to few 1000's of years) magmatic crystal residence (Davidson et al., 2001; Andrews et al., 2008). Comparatively frequent preservation of xenocrystic zircon in El Chichón magmas relative to many other continental arc volcanoes may reflect the early stages of a subvolcanic magma reservoir where assimilation of country rocks is possible whereas established magma systems are shielded from their host rocks by a carapace of precursor intrusions.

6. Conclusions

Although numerous studies have been made about El Chichón volcano, zircon has not yet been described, and consequently the discovery and dating of zircon via U–Th and U–Pb geochronology is important as it provides unique insights into the El Chichón magma system. This study specifically explores zircon ages from juvenile rocks (pumice and lava) from the 1982 eruption and selected antecedent eruptions dating back to ca. 1600 BP. U–Th isochron ages for El Chichón zircons range from late Holocene to ca. 84 ka, with hardly any resolvable differences between samples. In addition, secular equilibrium zircon domains with different properties in CCL are present which yielded heterogeneous U–Pb ages consistent with detrital provenance from regional metaigneous and metasedimentary sources. The spread of zircon ages suggests that magmatic activity at El Chichón had already initiated by ca. 84 ka, but there is no evidence for zircons similar in age to $^{40}Ar/^{39}Ar$ dates for some older accidental lithics and precursor domes. During the late Pleistocene–Holocene, a subvolcanic reservoir has formed whose boundary layer of crustally contaminated intrusions exerted strong control on the isotopic properties of the Holocene El Chichón magmas. Zircon is recycled from this reservoir during ephemeral recharge events which also may have interrupted intermittent eruptive dormancy.

Supplementary data to this article can be found online at http://dx.doi.org/10.1016/j.jvolgeores.2016.01.011.

Acknowledgements

Alejandro Cisneros provided support during field work, and helpful comments to earlier versions of the manuscript. Adriana Camacho is thanked for assistance during field work, and Mélanie Barboni for supervising zircon separation. We also thank the editor, Malcolm Rutherford, and reviewer Erik Klemetti for their constructive comments. Support through UC-MEXUS grant CN 13-567 and the Instrumentation and Facilities Program, Division of Earth Sciences, National Science Foundation, is acknowledged.

References

Annen, C., Wagner, J.J., 2003. The impact of volcanic eruptions during the 1990s. Nat. Hazard. Rev. 4 (4), 169–175.
Andrews, B.J., Gardner, J.E., Housh, T.B., 2008. Repeated recharge, assimilation, and hybridization in magmas erupted from El Chichón as recorded by plagioclase and amphibole phenocrysts. J. Volcanol. Geotherm. Res. 175 (4), 415–426.
Arce, J.L., Walker, J., Keppie, J.D., 2014. Petrology of two contrasting Mexican volcanoes, the Chiapanecan (El Chichón) and Central American (Tacaná) volcanic belts: the result of rift- *versus* subduction-related volcanism. Int. Geol. Rev. 56 (4), 501–524.
Arce, J.L., Walker, J., Keppie, J.D., 2015. Petrology and geochemistry of El Chichón and Tacaná: two active, yet contrasting Mexican volcanoes. Active Volcanoes of Chiapas (Mexico): El Chichón and Tacaná (pp. 25–43). Springer, Berlin Heidelberg.
Bacon, C.R., Persing, H.M., Wooden, J.L., Ireland, T.R., 2000. Late Pleistocene granodiorite beneath Crater Lake caldera, Oregon, dated by ion microprobe. Geology 28 (5), 467–470.
Bacon, C.R., Lowenstern, J.B., 2005. Late Pleistocene granodiorite source for recycled zircon and phenocrysts in rhyodacite lava at Crater Lake, Oregon. Earth Planet. Sci. Lett. 233 (3), 277–293.
Belousova, E.A., Griffin, W.L., Pearson, N.J., 1998. Trace element composition and cathodoluminescence properties of southern African kimberlitic zircons. Mineral. Mag. 62 (3), 355–366.
Boehnke, P., Watson, E.B., Trail, D., Harrison, T.M., Schmitt, A.K., 2013. Zircon saturation re-revisited. Chem. Geol. 351, 324–334.
Cherniak, D.J., Hanchar, J.M., Watson, E.B., 1997. Diffusion of tetravalent cations in zircon. Contrib. Mineral. Petrol. 127 (4), 383–390.
Claiborne, L.L., Miller, C.F., Flanagan, D.M., Clynne, M.A., Wooden, J.L., 2010. Zircon reveals protracted magma storage and recycling beneath Mount St. Helens. Geology 38 (11), 1011–1014.
Cooper, K.M., Kent, A.J., 2014. Rapid remobilization of magmatic crystals kept in cold storage. Nature 506 (7489), 480–483.
Craig, H., 1957. Isotopic standards for carbon and oxygen and correction factors for mass-spectrometric analysis of carbon dioxide. Geochim. Cosmochim. Acta 12 (1), 133–149.
Damon, P., Montesinos, E., 1978. Late Cenozoic volcanism and metallogenesis over an active Benioff Zone in Chiapas. Mexico. Ariz. Geol. Soc. Dig. 11, 155–168.
Davidson, J.P., Tepley, F.J., 1997. Recharge in volcanic systems: evidence from isotope profiles of phenocrysts. Science 275 (5301), 826–829.
Davidson, J., Tepley, F., Palacz, Z., Meffan-Main, S., 2001. Magma recharge, contamination and residence times revealed by in situ laser ablation isotopic analysis of feldspar in volcanic rocks. Earth Planet. Sci. Lett. 184 (2), 427–442.
Davidson, J.P., Morgan, D.J., Charlier, B.L., 2007. Isotopic microsampling of magmatic rocks. Elements 3 (4), 253–259.
De la Cruz-Reyna, S., Martin Del Pozzo, A.L., 2009. The 1982 eruption of El Chichón volcano, Mexico: eyewitness of the disaster. Geofis. Int. 48 (1), 21–31.
Duffield, W.A., Tilling, R.I., Canul, R., 1984. Geology of El Chichón Volcano, Chiapas, Mexico. J. Volcanol. Geotherm. Res. 20 (1-2), 117–132.
Espindola, J.M., Macias, J.L., Tilling, R.I., Sheridan, M.F., 2000. Volcanic history of El Chichón Volcano (Chiapas, Mexico) during the Holocene, and its impact on human activity. Bull. Volcanol. 62 (2), 90–104.
Fletcher, J.M., Grove, G., Kimbrough, D., Lovera, O., GE, G., 2007. Magdalena shelf and southern Gulf of California: insights from detrital zircon U–Pb ages from the Magdalena fan and adjacent areas. GSA Bull. 119 (11/12), 1313–1336 (Nov./Dec. 2007).
García-Palomo, A., Macías, J.L., Espíndola, J.M., 2004. Strike-slip faults and K-alkaline volcanism at El Chichón volcano southeastern México. J. Volcanol. Geotherm. Res. 136, 247–268.
Garrison, J., Davidson, J., Reid, M., Turner, S., 2006. Source versus differentiation controls on U-series disequilibria: insights from Cotopaxi Volcano, Ecuador. Earth Planet. Sci. Lett. 244 (3), 548–565.
Havskov, J., De la Cruz-Reyna, S., Singh, S.K., Medina, F., Gutiérrez, C., 1983. Seismic activity related to the March–April, 1982 eruptions of El Chichón Volcano, Chiapas, Mexico. Geophys. Res. Lett. 10 (4), 293–296.
Juvigné, E., 1983. Les variations minéralogiques dans les retombées de 1982 du volcan El Chichon (Chiapas, Mexique) et leur intérêt pour la téphrostratigraphie. Annales de la Société géologique de Belgique 106, 311–325.
Kim, Y.H., Clayton, R.W., Keppie, F., 2011. Evidence of a collision between the Yucatán Block and Mexico in the Miocene. Geophys. J. Int. 187, 989–1000.
Klemetti, E.W., Clynne, M.A., 2014. Localized rejuvenation of a crystal mush recorded in zircon temporal and compositional variation at the Lassen Volcanic Center, northern California. PLoS ONE 9 (12), e113157.
Layer, P.W., Garcia-Palomo, A., Jones, D., Macias, J.L., Arce, J.L., Mora, J.C., 2009. El Chichón volcanic complex, Chiapas, México: stages of evolution based on field mapping and $^{40}Ar/^{39}Ar$ geochronology. Geofis. Int. 48 (1), 33–54.
Luhr, J.F., Carmichael, I.S.E., Varekamp, J., 1984. The 1982 eruptions of El Chichón Volcano, Chiapas, Mexico: mineralogy and petrology of the anhydrite-bearing pumices. J. Volcanol. Geotherm. Res. 23, 69–108.

Luhr, J.F., 1990. Experimental phase relations of water-and sulfur-saturated arc magmas and the 1982 eruptions of El Chichón volcano. J. Petrol. 31 (5), 1071–1114.
Macías, J.L., Arce, J.L., Mora, J.C., Espíndola, J.M., Saucedo, R., Manetti, P., 2003. A 550-year-old Plinian eruption at El Chichón Volcano, Chiapas, Mexico: explosive volcanism linked to reheating of the magma reservoir. J. Geophys. Res. Solid Earth (1978–2012) 108 (B12).
Manea, M., Manea, V.C., 2008. On the origin of El Chichón volcano and subduction of Tehuantepec Ridge: a geodynamical perspective. J. Volcanol. Geotherm. Res. 175 (4), 459–471.
Matson, M., 1984. The 1982 El Chichón volcano eruptions—a satellite perspective. J. Volcanol. Geotherm. Res. 23, 1–10.
Müllerried, F.K.G., 1932. Der Chichón, ein bisher unbekannter tätiger Vulkan im nördlichen Chiapas. Mexiko: Zeitschrift für Vulkanologie 14, 191–209.
Olsson, I.U., 1986. Radiometric methods. In: Berglund, B. (Ed.), Handbook of Holocene palaeoecology and palaeohydrology. John Wiley & Sons, Chichester, pp. 273–312.
Pardo, M., Suarez, G., 1995. Shape of the subducted Rivera and Cocos Plates in southern Mexico: seismic and tectonic implication. J. Volcanol. Geotherm. Res. 100, 12357–12373.
Pickett, D.A., Murrell, M.T., Tilling, R.I., 1993. U/Th and Th isotopes in minerals from El Chichón trachyandesite: implications for crystal/liquid partitioning in andesitic systems. EOS Trans. Am. Geophys. Union 74 (16), 341.
Pickett, D.A., Murrell, M.T., 1997. Observations of $^{231}Pa/^{235}U$ disequilibrium in volcanic rocks. Earth Planet. Sci. Lett. 148, 259–271.
Rebollar, C.J., Espíndola, V.H., Uribe, A., Mendoza, A., Pérez-Vertti, A., 1999. Distribution of stress and geometry of the Wadati-Benioff zone under Chiapas, Mexico. Geofis. Int. 38, 95–106.
Reid, M.R., Coath, C.D., Harrison, T.M., McKeegan, K.D., 1997. Prolonged residence times for the youngest rhyolites associated with Long Valley Caldera: $^{230}Th–^{238}U$ ion microprobe dating of young zircons. Earth Planet. Sci. Lett. 150, 27–39.
Rose Jr., W.I., Bornhorst, T.J., Halso, S.P., Capaul, W.A., Plumley, P.S., Cruz-Reyna, S.D., Mena, M., Mota, R., 1984. Volcán El Chichón, Mexico: pre-1982 S-rich eruptive activity. J. Volcanol. Geotherm. Res. 23 (147-149), 155–167.
Rudnick, R.L., Gao, S., 2004. Composition of the continental crust. In: Holland, H.D., Turekian, K.K. (Eds.), Treatise on Geochemistry vol. 3. Elsevier, Amsterdam, pp. 1–64.
Samperton, K.M., Schoene, B., Cottle, J.M., Keller, C.B., Crowley, J.L., Schmitz, M.D., 2015. Magma emplacement, differentiation and cooling in the middle crust: integrated zircon geochronological–geochemical constraints from the Bergell Intrusion, Central Alps. Chem. Geol. 417, 322–340.
Schmitt, A.K., Grove, M., Harrison, T.M., Lovera, O., Hulen, J., Walters, M., 2003. The Geysers-Cobb Mountain Magma System, California (Part 1): U–Pb zircon ages of volcanic rocks, conditions of zircon crystallization and magma residence times. Geochim. Cosmochim. Acta 67 (18), 3423–3442.
Schmitt, A.K., 2011. Uranium series accessory crystal dating of magmatic processes. Annu. Rev. Earth Planet. Sci. 39, 321–349.
Schmitt, A.K., Danišík, M., Aydar, E., Şen, E., Ulusoy, İ., Lovera, O.M., 2014. Identifying the volcanic eruption depicted in a Neolithic painting at Çatalhöyük, Central Anatolia, Turkey. PLoS ONE 9 (1). http://dx.doi.org/10.1371/journal.pone.0084711.
Scolamacchia, T., Capra, L., 2015. El Chichón Volcano: eruptive history. Active Volcanoes of Chiapas (Mexico): El Chichón and Tacaná (pp. 45–76). Springer, Berlin Heidelberg.
Stelten, M.E., Cooper, K.M., 2012. Constraints on the nature of the subvolcanic reservoir at South Sister volcano, Oregon from U-series dating combined with sub-crystal trace-element analysis of plagioclase and zircon. Earth Planet. Sci. Lett. 313, 1–11.
Stuiver, M., Polach, H.A., 1977. Discussion; reporting of C-14 data. Radiocarbon 19 (3), 355–363.
Tepley, F.J., Davidson, J.P., Tilling, R.I., Arth, J., 2000. Magma mixing, recharge and eruption histories in plagioclase phenocrysts from El Chichón Volcano, Mexico. J. Petrol. 41, 1397–1411.
Tilling, R.I., Rubin, M., Sigurdsson, H., Carey, S., Duffield, W.A., 1984. Prehistoric eruptive activity of El Chichón volcano, Mexico. Science 224, 747–749.
Varekamp, J.C., Luhr, J.F., Prestegaard, K.L., 1984. The 1982 eruptions of El Chichón Volcano (Chiapas, Mexico): character of the eruptions, ash-fall deposits, and gasphase. J. Volcanol. Geotherm. Res. 23 (1), 39–68.
Walker, B.A., Grunder, A.L., Wooden, J.L., 2010. Organization and thermal maturation of long-lived arc systems: evidence from zircons at the Aucanquilcha volcanic cluster, northern Chile. Geology 38 (11), 1007–1010.
Watson, E.B., 1996. Dissolution, growth and survival of zircons during crustal fusion: kinetic principles, geological models and implications for isotopic inheritance. Geol. Soc. Am. Spec. Pap. 315, 43–56.
Weber, B., Valencia, V.A., Schaaf, P., Pompa-Mera, V., Ruiz, J., 2008. Significance of provenance ages from the Chiapas Massif Complex (southeastern Mexico): redefining the Paleozoic basement of the Maya Block and its evolution in a peri-Gondwanan realm. J. Geol. 116 (6), 619–639.
Weber, B., Valencia, V.A., Schaaf, P., Ortega-Gutiérrez, F., 2009. Detrital zircon ages from the Lower Santa Rosa Formation, Chiapas: implications on regional Paleozoic stratigraphy. Rev. Mex. Cienc. Geol. 26 (1), 260–276.